Pharmaceutical Research, Vol. 26, No. 10, October 2009 (© 2009)
DOI: 10.1007/s11095-009-9945-8

Research Paper

Role of Convective Flow in *Carmustine* Delivery to a Brain Tumor

Davis Yohanes Arifin,[1] Kam Yiu Timothy Lee,[2] Chi-Hwa Wang,[1,3,5] and Kenneth A. Smith[1,4]

Received March 13, 2009; accepted July 14, 2009; published online July 29, 2009

Purpose. This paper presents a three-dimensional patient-specific simulation of *carmustine* delivery to brain tumor. The simulation investigates several crucial factors, particularly the role of convective flow, affecting drug delivery efficacy.
Methods. The simulation utilizes a complete three-dimensional tissue geometry constructed from magnetic resonance images (MRI) of a brain tumor patient in whom commercially available Gliadel® wafers were implanted for sustained delivery of *carmustine* following excision of the tumor. This method permits an estimation of the convective flow field (in the irregularly shaped anatomical region) which can be used for prediction of drug penetration into the domain of interest, i.e. remnant tumor. A finite volume method is utilized to perform all simulations.
Results. Drug exposure exceeds its threshold therapeutic concentration (~15 μM) but for only a limited time (i.e. less than a week) and only in the immediately adjacent tissue (i.e. less than 2 mm). A quasi-steady transport process is established within 1 day following treatment, in which the drug is eliminated rapidly by transcapillary exchange, while its penetration into the tumor is mainly by diffusion. Convection appears to be crucial in influencing the drug distribution in the tumor: the remnant tumor near the ventricle is, by one to two orders of magnitude, less exposed to the drug than is the distal remnant tumor.
Conclusions. *Carmustine* penetration from Gliadel® wafers implanted in brain is limited by rapid elimination via transcapillary exchange. Therefore, it could be useful to consider other therapeutic agents such as *paclitaxel*. In addition, local convective flow within the cavity appears to be a crucial factor in distributing the drug so that the tumor domain near the ventricle is prone to minimal drug exposure. Thus, complete removal of the tumor from this region is of particular concern.

KEY WORDS: BCNU; computational fluid dynamics; convection; diffusion; Gliadel® wafer; *glioblastoma*.

INTRODUCTION

In 2006, an estimated 19,000 new cases of brain tumors and 13,000 deaths were reported in the United States (1). This accounts for about 1.4% of all cancer cases and 2.3% of all cancer cases that cause death. Upon diagnosis, brain tumor size typically varies between 10 and 100 cm^3, equivalent to approximately 1–10 × 10^{10} tumor cells. To have the immune system control the malignancy, the number of tumor cells must be reduced to approximately 10^5 cells (2). The most common current strategy against brain tumors is a combination of surgical removal, chemotherapy, and

[1] Molecular Engineering of Biological and Chemical Systems (MEBCS), Singapore-MIT Alliance, 4 Engineering Drive 3, Singapore, 117576, Singapore.
[2] Gleneagles Hospital Ltd, 6A Napier Road, Singapore, 258500, Singapore.
[3] Department of Chemical and Biomolecular Engineering, National University of Singapore, 4 Engineering Drive 4, Singapore, 117576, Singapore.
[4] Department of Chemical Engineering, Massachusetts Institute of Technology, Cambridge, Massachusetts 02139, USA.
[5] To whom correspondence should be addressed. (e-mail: chewch@nus.edu.sg)

NOTATIONS: α, Volume fraction of interstitial/extracellular space; α^T, Volume fraction of interstitial/extracellular space in the remnant tumor; α^N, Volume fraction of interstitial/extracellular space in the normal tissue; α*, Retardation constant; α^{*T}, Retardation constant in the remnant tumor; α^{*N}, Retardation constant in the normal tissue; β, Volume fraction of intracellular space; ξ, Dimensionless distance from cavity/remnant tumor interface (x/L_d); ξ^N, Dimensionless distance from the surface of polymer pellet (x^N/L_d^N); γ, Ratio of conductivity of Darcy's permeability in the cavity and the tissue, K^C/K^N; Γ, Dimensionless drug concentration relative to effective concentration ($C_i/C_{i,eff}$); Γ_T, Dimensionless drug concentration relative to that at the cavity/remnant tumor interface ($C_i/C_{i,c}$); Γ_N, Dimensionless drug concentration relative to that at the surface of polymer pellet as no cavity is present ($C_i/C_{i,c}^N$); μ, Viscosity of the interstitial fluid (Pa-s); π_i, Interstitial osmotic pressure (Pa); π_v, Vascular osmotic pressure (Pa); ρ, Density of the interstitial fluid (kg/m^3); ψ, Constant to determine the importance of convection in the remnant tumor; ψ^N, Constant to determine the importance of convection in the normal tissue; ϕ, Thiele modulus in the cavity; σ, Osmotic reflection coefficient of plasma; τ, Dimensionless time relative to the first-order elimination constant in the tissue; B, Average bound drug concentration (M); B_i, Bound drug concentration in the interstitial phase (M); B_c, Bound drug concentration in the intracellular phase (M); B_m, Bound drug concentration in the cell membrane phase (M); C, Average free drug concentration (M); C_i, Free drug concentration in the interstitial phase (M); C_c, Free drug concentration in the

radiotherapy (2). The combination of surgery and radiotherapy may produce a 1,000-fold reduction; therefore, chemotherapy must achieve a 100–1,000 fold tumor cell reduction (2).

However, drug delivery by systemic administration faces numerous problems (3–5), not the least of which is the blood brain barrier (BBB). Current practice therefore favors a localized strategy which bypasses the BBB by the insertion of polymeric drug carriers into the cavity produced by surgical removal of the tumor. These carriers provide for the sustained release of therapeutic agents directly into the tumor site. For brain tumors, the Gliadel® wafer was approved by the FDA in 1996 as an adjuvant therapy (6). Each wafer is made from the biodegradable polymer PCPP/SA *(poly (carboxyphenoxy-propane/sebacic acid))* and has a diameter of 14 mm and a thickness of 1 mm. The mass of a single wafer is 200 mg, and each contains 3.85% *carmustine*. The number of wafers implanted in the surgical cavity is limited to eight. This achieves a total dosage of 61.6 mg of *carmustine.* A Phase II clinical trial of Gliadel® revealed that the median survival time increased minimally from 11.6 months to 13.0 months in 240 newly diagnosed malignant *glioma* patients (6). A recent long-term trial has shown that malignant *glioma* patients treated with *carmustine* as an adjuvant to surgery and radiotherapy enjoy a survival advantage at 2 and 3 years post-op as compared to those who received a placebo (7). Of 59 patients involved in this study, 11 were alive at 56 months. Of those, nine had been treated with Gliadel® wafers and two with placebo wafers. However, a different study has shown that implantation of these wafers does not help reduce the pattern of recurrence (8). Therefore, it seems that implantation of Gliadel® wafers does improve the clinical outcome, but not dramatically. These observations have motivated this study, which attempts to understand why local drug delivery may not lead to an optimal clinical outcome despite all of its inherent advantages.

Thus, the aim of this study is to evaluate the performance of *carmustine* delivery from Gliadel® wafers via a computer simulation. In the present study, a three-dimensional patient-specific model is presented to address the overall effect of brain interstitial fluid flow. Here, the geometry is constructed from MRI images of a patient with *glioblastoma*. The brain interstitial fluid flow field is estimated by computational fluid dynamic (CFD) methods for a variety of conditions. The results are then used to predict the role of convection on drug distribution within the cavity and in the tissue. Subsequently, a simple one-dimensional model is developed to elucidate *carmustine* distribution within the tissue, provided that the drug concentration on the surface of the cavity is known.

SIMULATION MODEL

Patient Model Geometry

The geometry was obtained from magnetic resonance images (MRI) of a patient with a *glioblastoma* tumor (courtesy of The Brain and Spine Clinic, Gleneagles Hospital, Singapore). The MRI was reconstructed into connected surface grids by Mimics 10 (Materialise Inc, 2006). A pre-processor grid generator (Gambit 2.3.16, ANSYS Inc., 2006) was then utilized to generate 3D volume grids and interfaces for the simulation. This technique is able to reconstruct brain geometry with a precision of ±3 mm. The model geometry is shown in Fig. 1. The typical simulation comprises about 11,000,000 tetrahedral elements, located mainly in the vicinity of wafer implantation. Such a high grid density is necessary due to the transport properties of *carmustine,* i.e. rapid transcapillary elimination. Calculations are performed by utilizing commercial computational fluid dynamics (CFD) software (Fluent 6.3.26, ANSYS Inc., 2006).

Our previous work, which was focused on different drugs, employed a simple isolated tumor model (9–11); however, a full brain model is necessary to capture the overall interstitial fluid flow. The total flow rate of interstitial fluid in human brain is about 5.83×10^{-6}kg/s (12,13), 70% of which is contributed by the ventricle, while the remainder originates from the capillaries. The innermost boundary condition is on the ventricle surface where interstitial fluid is constantly infused at constant pressure ($p_{\text{ventricle}} = 1447.4$ Pa), while the outermost boundary condition is the pressure at the *arrachnoid villi* ($p_{\text{outer}} = 657.9$ Pa) on the outermost surface of the brain where the fluid is removed (12). In contrast, there

intracellular phase (M); C_m, Free drug concentration in the cell membrane phase (M); $C_{i,c}$, Free interstitial drug concentration at the cavity/remnant tumor interface (M); $C_{i,c}^N$, Free interstitial drug concentration at the surface of polymer pellet (M); $C_{i,eff}$, Free effective interstitial drug concentration (M); D, Lumped diffusion coefficient in the tissue (m^2/s); D^T, Lumped diffusion coefficient in the remnant tumor (m^2/s); D^N, Lumped diffusion coefficient in the normal tissue (m^2/s); D_i, Diffusion coefficient in interstitial phase (m^2/s); F_V, Rate of fluid gain from the capillary blood flow per unit volume of tissue (1/s); L, Average thickness of the remnant tumor (m); L_{brain}, Average radius of the brain (m); L_c, Characteristic length scale of the cavity (m); L_d, Diffusion/reaction length scale in the tissue (m); L_d^T, Diffusion/reaction length scale in the remnant tumor (m); L_d^N , Diffusion/reaction length scale in the normal tissue (m); L_p, Hydraulic conductivity in the tissue (m/Pa/s); L_p^T, Hydraulic conductivity in the remnant tumor (m/Pa/s); L_p^N, Hydraulic conductivity in the normal tissue (m/Pa/s); k, Lumped first-order elimination constant in the tissue (1/s); k^T, Lumped first-order elimination constant in the remnant tumor (1/s); k^N, Lumped first-order elimination constant in the normal tissue (1/s); k_{bbb}, Elimination constant to blood capillaries (1/s); k_c, Elimination constant in the cavity (1/s); k_e, Elimination constant due to enzymatic/non-enzymatic reactions (1/s); K, Darcy's permeability in the tissue (m^2); K^C, Darcy's permeability in the cavity (m^2); K^T, Darcy's permeability in the remnant tumor (m^2); K^N, Darcy's permeability in the normal tissue (m^2); K_c, Binding constant between free and bound drugs in intracellular phase; K_i, Binding constant between free and bound drugs in interstitial phase; p_i, Interstitial fluid pressure (Pa); p_v, Vascular pressure (Pa); p_{outer}, Pressure at the *arrachnoid villi* on the outermost surface of the brain (Pa); $p_{ventricle}$, Pressure on the ventricle surface (Pa); $P_{c/i}$, Partition coefficient between cellular and interstitial phase; $P_{m/i}$, Partition coefficient between membrane and interstitial phase; Pe_c, Peclet number in the cavity; Pe_t, Peclet number in the tissue, e.g. tumor; R, Average radius of the intact tumor (m); Re, Reynolds number; S/V, Blood vessel exchange area in the tissue (m^{-1}); S/V^T, Blood vessel exchange area in the remnant tumor (m^{-1}); S/V^N, Blood vessel exchange area in the normal tissue (m^{-1}); t, Time (s); $\mathbf{v}$, Interstitial fluid velocity vector (m/s); v_s, Characteristic fluid velocity in the tissue (m/s); $v_{s,c}$, Characteristic fluid velocity in the cavity (m/s); v_x, Characteristic fluid velocity at the cavity/remnant tumor interface (m/s); x, Distance from cavity/remnant tumor interface (m); x^N, Distance from polymer pellet surface (m).

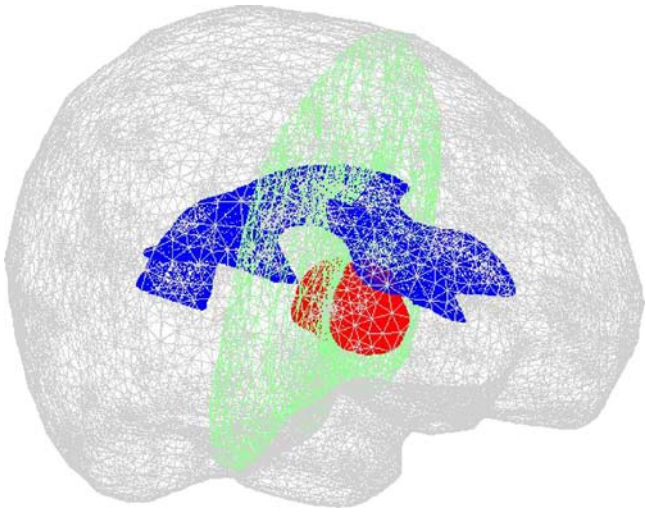

Fig. 1. The model geometry used from a brain tumor patient, showing the presence of ventricle (shown in *blue*), tumor (*red*) located in temporal lobe, and remaining normal brain tissue. The coronal surface (*green*) is used for representative 2D surface visualization throughout this study.

are no appropriate boundary conditions available for the isolated tumor model, as they will vary depending on tumor location. In order to simplify the simulation geometry, the model presented here does not distinguish between white and gray matter. Given the short penetration of *carmustine* into the thin layer (several mm) around the cavity, the white and gray matter differentiation is not important from that perspective. It may somewhat influence interstitial flow, but the separate permeabilities for the two domains are not known, so a single value was utilized. In addition, our model also does not consider the poroelastic properties of brain tissue. The cavity domain might deform following the surgery, but data on this topic are not available.

Fig. 2a shows the coronal geometry with the tumor present. The tumor volume is 12.8 cc, which is considered small, giving an equivalent spherical mean radius (R) of 14.5 mm. The tumor is surgically removed, leaving a cavity in the core and surrounding residual tumor with an average thickness (L) of 2.3 mm. Subsequently, eight Gliadel® wafers are inserted into the open cavity. The wafers are held in place by surgical cellulose (Surgicel). Fig. 2b depicts the 3D geometry of the tumor site following surgery and implantation of the eight wafers.

Transport Model

The transport of interstitial fluid in the brain is described by coupling the modified continuity and momentum equations for fluid flow in a porous medium (14). The interstitial fluid is assumed to be water at 37°C. Table I provides the baseline values of parameters related to the flow. When applicable, superscripts C, T, and N correspond to parameter values in the cavity, the remnant tumor, and the normal brain tissue. The continuity equation for incompressible interstitial fluid in the brain tissue is

$$\nabla \cdot \mathbf{v} = F_V \tag{1}$$

where $\mathbf{v}$ is superficial fluid velocity vector and F_V is the rate of fluid gain from the capillary blood flow per unit volume of tissue. Fluid removal by the lymphatic system is not included because brain tissue lacks a well-defined lymphatic system. The fluid gain is assumed to be a non-uniformly distributed source, depending on the pressure difference between blood vessels and interstitial fluid. The constitutive equation for F_V follows Starling's law (15):

$$F_V = L_p(S/V)[p_V - p_i - \sigma(\pi_V - \pi_i)] \tag{2}$$

where L_p is hydraulic conductivity of the microvascular wall, p_V is vascular pressure, p_i is interstitial fluid pressure, S/V is available exchange area of the blood vessels per unit volume of tissue, σ is the osmotic reflection coefficient for plasma proteins, and π_V and π_i are osmotic pressures of blood plasma and interstitial fluid, respectively.

Surgical resection often leads to brain tissue trauma and causes damage to the BBB, giving rise to a significant increase in the hydraulic conductivity of the blood capillaries (16–18). The phenomenon is known as traumatic brain edema, in which fluid production may increase by 10–100 fold. This results in fluid accumulation and relatively high pressures in the cavity and surrounding remnant tumor domains. However, the magnitude and time course of edema

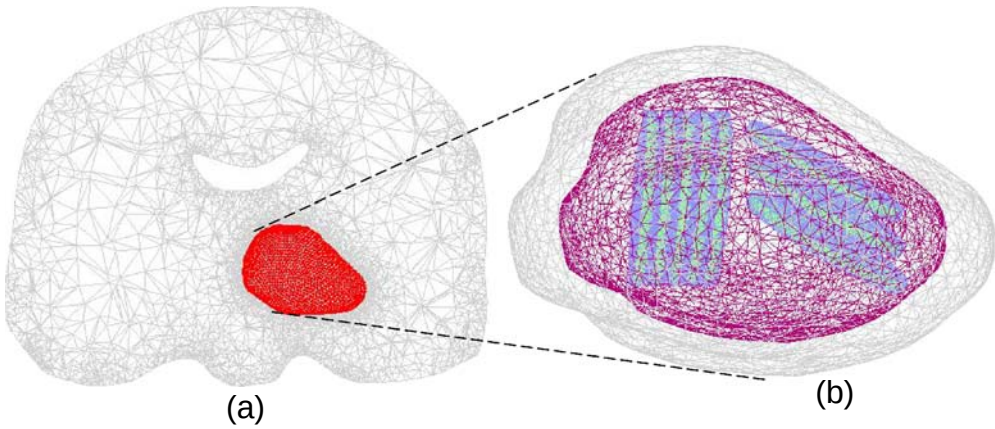

Fig. 2. **a** The coronal sectional of the brain (shown *green* in Fig. 1) with the treatment domain (*red*); **b** the 3D treatment domain with eight Gliadel® wafers (*light green* with *blue line*), cavity (*dark red*), and remnant tumor (*gray*).

Table I. Interstitial Fluid-Related Parameter Values

	Parameter	Cavity	Remnant tumor	Normal tissue
ρ	Density of the interstitial fluid (kg/m^3)	1,000 (24)	1,000 (24)	1,000 (24)
μ	Viscosity of the interstitial fluid (Pa-s)	7×10^{-4} (24)	7×10^{-4} (24)	7×10^{-4} (24)
p_v	Vascular pressure (Pa)	N/A	4,610 (12)	4,610 (12)
S/V	Blood vessel exchange area (m^{-1})	N/A	20,000 (15)	7,000 (15)
π_v	Vascular osmotic pressure (Pa)	N/A	3,440 (12)	3,440 (12)
π_i	Interstitial osmotic pressure (Pa)	N/A	1,110 (15)	740 (15)
σ	Osmotic reflection coefficient of plasma	N/A	0.82 (15)	0.91 (15)
L_p	Hydraulic conductivity (m/Pa/s)	N/A	1.1×10^{-12}	1.4×10^{-13}
K	Darcy's permeability (m^2)	1×10^{-11}	6.4×10^{-14}	6.4×10^{-15}

may vary depending on the extent of surgery and the recovery capability of the patient. Furthermore, detailed data are scarce. Thus, the dynamics of edema are a matter of controversy. Nevertheless, it is a common fact that edema due to traumatic injury will emerge immediately and resolve in about a 3-day to 1-week period (17–20). In this simulation, the variation of hydraulic conductivity with time is modified from previous work (11) to account for its resolution. It is also assumed that the hydraulic conductivity of remnant tumor (L_p^T) is uniformly affected by edema, but that no other tissue is affected. The current model utilizes the following equation:

$$L_p^T(t) = L_p^T(t=0)[1 + a\exp(-bt)] \tag{3}$$

where t is time in seconds and a and b are constants, taken to be 9 and 1.94×10^{-5} 1/s, respectively. With this choice of constants, tumor hydraulic conductivity is 94% resolved at 3 days and 99.99% resolved at 1 week.

The brain tissue is assumed to be a rigid porous medium. The momentum equation for fluid flow through tissue is assumed to be

$$\rho\left(\frac{\partial \mathbf{v}}{\partial t} + \mathbf{v}\cdot\nabla\mathbf{v}\right) = -\nabla p_i + \mu\nabla^2\mathbf{v} - \left(\frac{\mu}{K}\right)\mathbf{v} \tag{4}$$

where t is time, ρ and μ are density and viscosity of the interstitial fluid, and K is the Darcy permeability of the tissue.

The dimensionless forms of the equations of continuity and motion are then as follows:

$$\widetilde{\nabla}\cdot\tilde{\mathbf{v}} = \widetilde{F_V} \tag{5}$$

$$\frac{\partial\tilde{\mathbf{v}}}{\partial\tau} + \tilde{\mathbf{v}}\cdot\widetilde{\nabla}\tilde{\mathbf{v}} = -\frac{(p_{ventricle} - p_{outer})}{\rho v_s^2}\widetilde{\nabla}\tilde{p_i} + \frac{1}{\mathrm{Re}}\widetilde{\nabla}^2\tilde{\mathbf{v}} - \frac{1}{\mathrm{Re}}\left(\frac{{L_{brain}}^2}{K}\right)\tilde{\mathbf{v}} \tag{6}$$

where $\widetilde{\nabla} = L_{brain}\nabla$, and L_{brain} is the mean radius of the brain, i.e. 70 mm, which has been chosen as the characteristic length scale, $\tilde{\mathbf{v}} = \mathbf{v}/v_s$ ($v_s = (K^N/\mu)(p_{ventricle} - p_{outer})/L_{brain} = 1\times10^{-7}$m/s is the velocity scale), $\tau = t/(L_{brain}/v_s)$, $\tilde{p_i} = (p_i - p_{outer})/(p_{ventricle} - p_{outer})$ is the dimensionless pressure difference (relative to p_{outer}) over the pressure difference between $p_{ventricle}$ and p_{outer}, $\widetilde{F_V} = F_V/(v_s/L_{brain})$ is the dimensionless fluid gain rate from vessel permeation, and $\mathrm{Re} = \rho L_{brain} v_s/\mu$ is the Reynolds number. Insertion of parameter values from Table I leads to the conclusion that Eq. 6 can be further simplified to

$$\tilde{\mathbf{v}} = -\widetilde{\nabla}\tilde{p_i} \tag{7}$$

Drug is always present in two different forms: free and bound; the latter is usually not subject to metabolism (19). Furthermore, brain tissue consists of three phases: interstitial/extracellular space (ECS), intracellular space (ICS), and cell membrane (CM) (20–22). Both forms of drug are distributed amongst these three phases. The average concentrations can be expressed as follows:

$$C = \alpha C_i + \beta C_c + (1-\alpha-\beta)C_m \tag{8}$$

$$B = \alpha B_i + \beta B_c + (1-\alpha-\beta)B_m \tag{9}$$

where C is the average free drug concentration; C_i, C_c, and C_m are the free drug concentrations in the interstitial, intracellular, and cell membrane spaces; while α and β are the volume fractions of interstitial and cellular spaces. The definition of bound drug is analogous to that for free drug: B is the average bound drug concentration; B_i, B_c, and B_m are the bound drug concentrations in the interstitial, intracellular, and cell membrane spaces. It is further assumed that the drug is neither eliminated nor bound in the membrane phase ($B_m = 0$).

In tissue, *carmustine* availability is dependent on the rate of transport (diffusion and convection), elimination (via blood capillaries and metabolism/degradation), and local binding (20–22). In the interstitial phase, the protein/fat-bound drug is assumed to be locally immobilized as it tends to immediately interact with cell/membrane surfaces due to its lipophilicity; therefore, only unbound drug is available for transport (19). Thus, the drug conservation equation, to be coupled to the flow equations, is as follows (20–22):

$$\frac{\partial C}{\partial t} = \alpha D_i\nabla^2 C_i - \nabla\cdot(\mathbf{v}C_i) - \alpha(k_{bbb} + k_e)C_i - \beta k_e C_c - \frac{\partial B}{\partial t} \tag{10}$$

where D_i is drug diffusivity in the interstitial space, k_{bbb} is the first-order elimination constant for drug transport through the BBB, and k_e is the enzymatic/non-enzymatic elimination constant due to metabolism/degradation. Table II provides all parameter values related to *carmustine*.

Table II. *Carmustine*-Related Parameter Values

	Parameter	Cavity	Remnant tumor	Normal tissue
α	Volume fraction of interstitial/extracellular space	1.00	0.35 (25)	0.20 (25)
β	Volume fraction of intracellular space	0.00	0.55 (21)	0.65 (21)
$P_{c/i}$	Partition coefficient between cellular and interstitial phase	N/A	1.00 (21)	1.00 (21)
$P_{m/i}$	Partition coefficient between membrane and interstitial phase	N/A	10.28 (21)	10.28 (21)
K_i, K_c	Binding constant between free and bound drugs	N/A	5.00 (21)	5.00 (21)
D_i	Diffusion coefficient in interstitial phase (m^2/s)	14.9×10^{-10} (23)	14.9×10^{-10} (23)	14.9×10^{-10} (23)
k_{bbb}	Elimination constant to blood capillaries (1/s)	N/A	1.44×10^{-2} (21)	1.44×10^{-2} (21)
k_c	Elimination constant in the cavity (1/s)	9.63×10^{-5} (26)	N/A	N/A
k_e	Elimination constant due to enzymatic/non-enzymatic reactions (1/s)	N/A	1.05×10^{-4} (21)	1.05×10^{-4} (21)
D	Lumped diffusion coefficient (m^2/s)	14.9×10^{-10}	7.8×10^{-11}	4.3×10^{-11}
k	Lumped first-order elimination constant (1/s)	9.63×10^{-5}	7.9×10^{-4}	4.4×10^{-4}

Several further assumptions are invoked to simplify the drug transport equation: (1) the bound drug concentrations in the interstitial (B_i) and intracellular phases (B_c) are directly proportional to those of the free drug (C_i and C_c), i.e. $K_i=B_i/C_i$ and $K_c=B_c/C_c$ where K_i and K_c are binding constants and (2) the free drug present in the three phases is in local equilibrium and the partitioning is linear so that $P_{c/i}=C_c/C_i$ and $P_{m/i}=C_m/C_i$. Note that, with these assumptions and transport data from Table II, the average concentration (C) becomes proportional to the concentration in the interstitial phase (C_i): $C=1.9C_i$ and $C=2.4C_i$ in tumor and normal brain tissue, respectively.

Furthermore, the convection term, i.e. $\nabla\cdot(\mathbf{v}C_i)$, is comprised of two sub-terms: the first, containing the gradient of concentration, is the usual convective term ($\mathbf{v}\cdot\nabla C_i$), while the second, containing the gradient of fluid velocity, is the dilution term ($C_i\nabla\cdot\mathbf{v}$). The latter can be simplified by Eq. 1 to become a sort of first-order elimination term, i.e. $F_V C_i$. However, *carmustine* is known to have a high transcapillary elimination rate constant (k_{bbb}) due to its high lipid solubility. For typical interstitial pressures and normal tissue, dilution is about three orders of magnitude less important than transcapillary elimination. Even in tumor tissue with severe edema, dilution is about two orders of magnitude less important than transcapillary elimination. Furthermore, while $P_{c/i}\approx 1$ (assuming water to be the main component in both interstitial and intracellular fluid), the enzymatic/non-enzymatic elimination term is also about two orders of magnitude less than k_{bbb} in both tumor and normal tissue. As a result, transcapillary exhange is the dominant sink for the drug. Finally, the drug conservation equation becomes

$$\frac{\partial C_i}{\partial t}=\left(\frac{\alpha}{\alpha^*}\right)D_i\nabla^2 C_i-\left(\frac{1}{\alpha^*}\right)\mathbf{v}\cdot\nabla C_i-\left(\frac{\alpha}{\alpha^*}\right)k_{bbb}C_i \qquad (11)$$

where $\alpha^*=\alpha(1+K_i)+\beta P_{c/i}(1+K_c)+(1-\alpha-\beta)P_{m/i}$ acts as a retardation constant for transport due to local binding and cell membrane partitioning. In the simplest form, this equation follows the simple diffusion/convection/reaction equation, i.e.

$$\frac{\partial C_i}{\partial t}=D\nabla^2 C_i-\mathbf{v}^*\cdot\nabla C_i-kC_i \qquad (12)$$

where $D=(\alpha/\alpha^*)D_i$ is the apparent diffusion coefficient in the brain tissue, $\mathbf{v}^*=\mathbf{v}/\alpha^*$ is the apparent interstitial fluid velocity vector in the brain tissue, and $k=\alpha k_{bbb}/\alpha^*$ is the apparent first-order elimination constant. In dimensionless form, Eq. 12 can be rewritten as

$$\frac{\partial\Gamma}{\partial\tau}=\widetilde{\nabla}^2\Gamma-\mathrm{Pe}_t\widetilde{\mathbf{v}}\cdot\widetilde{\nabla}\Gamma-\Gamma \qquad (13)$$

where $\Gamma=C_i/C_{i,eff}$ is dimensionless drug concentration relative to the effective therapeutic concentration ($C_{i,eff}$=15 μM, 22), $\widetilde{\mathbf{v}}=\mathbf{v}/v_s$ is the dimensionless interstitial fluid velocity, $\mathrm{Pe}_t=v_s L_d/\alpha^* D$ is a Peclet number that measures the importance of drug convection relative to diffusion in tissue, $L_d=\sqrt{D/k}$ is the diffusion/reaction length scale in the tissue, and $\tau=tk$ is the dimensionless time relative to the first-order elimination constant in the tissue (k). L_d in the remnant tumor ($L_d^T=\sqrt{D^T/k^T}$) is 0.31 mm, and the non-dimensional thickness of the remnant tumor (L/L_d^T) is 7.4. The remnant tumor is therefore "thick" and not very accessible to *carmustine*. The role of convection is determined by the magnitude of Pe_t. Taking the characteristic velocity to be $v_s=1\times10^{-7}$ m/s in both remnant tumor and nearby normal tissue, the value of Pe_t is 0.06 and 0.11, respectively, suggesting that in the tumor tissue the contribution of convection is modest as compared to diffusion.

In the cavity, all of the drug is in the "interstitial" phase and is available for transport. Binding and partitioning are assumed to be negligible, so that diffusion and convection take place without any restrictions. Hence, the drug transport follows the diffusion/convection/reaction equation in the interstitial medium:

$$\frac{\partial C_i}{\partial t}=D_i\nabla^2 C_i-\mathbf{v}\cdot\nabla C_i-k_c C_i \qquad (14)$$

where D_i is the diffusion coefficient in the interstitial phase, $\mathbf{v}$ is the fluid velocity vector, and $k_c=9.63\times10^{-5}$ 1/s (26) is the first-order degradation constant in the cavity. In the cavity, $\mathrm{Pe}_c=v_{s,c}L_c/D_i$ is a Peclet number that measures the importance of drug convection relative to diffusion in the cavity, $\phi=L_c\sqrt{k_c/D_i}$ is a Thiele modulus that is the ratio of the drug elimination rate to the diffusional transport rate, L_c (= 1 cm) is the cavity size length scale, and $v_{s,c}$ is the velocity length scale in the cavity. Selection of $v_{s,c}$ was guided by considering a spherical cavity of high conductivity (K^C) immersed in an ambient tissue of low conductivity (K^N). Far from the sphere, the pressure gradient was taken to be

everywhere uniform. The ratio of fluid fluxes in the two domains is $3\gamma/(2+\gamma)$ (27), where γ is the ratio of the conductivities, K^C/K^N. When γ becomes large, the ratio of the fluxes is simply 3. Therefore, the cavity velocity scale is approximately three times that in the tissue, i.e. $v_{s,c} = 3 \times 10^{-7}$ m/s. With these choices, $\phi = 2.5$ and $Pe_c = 2$, suggesting that drug degradation is mainly balanced by convection. Thus, a quasi-steady concentration in the cavity can be achieved in a time of about $L_c/v_{s,c}$, which is 9 h.

Eight Gliadel® wafers delivering a total *carmustine* dosage of 61.6 mg are implanted inside the cavity following the tumor removal surgery. Each wafer is assumed to be a solid porous medium with permeability of 3×10^{-13}m^2 (10,11). This permeability is much lower than that in the enveloping cavity region (1×10^{-11}m^2, (10,11)), causing the interstitial fluid to preferentially flow around the wafers. The drug release is assumed to be spatially uniform over the surface of the wafer. The release is temporally in accordance with the *in vivo* release kinetics in normal rat brain (20) as shown in Fig. 3. This shows an initial burst of about 70% of the total loading during the first 24 h, followed by a nearly constant release rate until 120 h. In addition, boundary conditions for all simulation studies include the continuity of drug flux across all internal boundaries. The concentrations of *carmustine* on ventricle and outer brain boundaries are set to zero.

RESULTS AND DISCUSSION

Fluid Flow Simulation of Brain Tumor Patient

The fluid flow in the brain is rather unique—it involves fluid permeation from the ventricle and from the blood vasculature. Therefore, a three-dimensional analysis with accurate geometry of the brain and tumor is required. We first simulate the normal brain fluid flow and then analyze the changes associated with the presence of tumor. In the former case, with the available literature data (the pressure boundary conditions and the magnitudes of interstitial fluid flow), we can estimate the two parameters (these parameters are known only within a wide range of reported values), namely Darcy's permeability (K^N) and hydraulic conductivity (L_p^N) of normal brain tissue. In the next section, we determine the flow field after most of the tumor has been surgically removed.

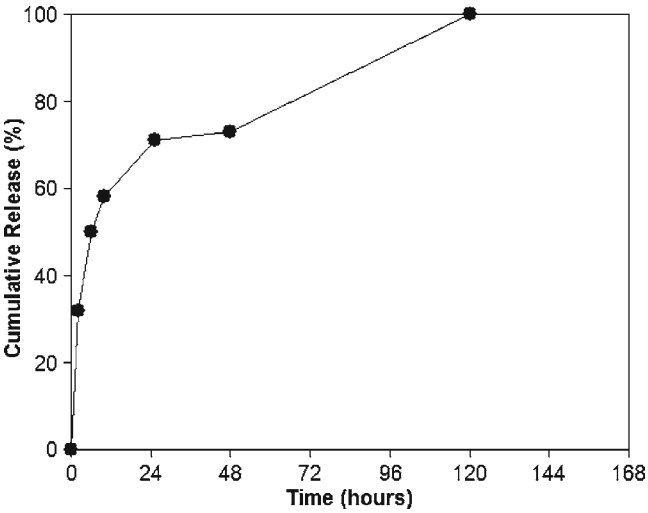

Fig. 3. Gliadel® *in vivo* release kinetics in normal rat brains (20).The Gliadel® release profile shows an initial 24 h burst which accounts for about 70% of the total loading, followed by a reasonably constant release rate until completion at Hour 120 (reprinted from (20) with permission from Wolters Kluwer).

Estimation of Darcy's Permeability (K^N) and Hydraulic Conductivity (L_p^N)

It is known that total interstitial fluid flow rate in the brain is 0.35 ml/min. Of this, 0.245 ml/min arises from the ventricles and 0.105 ml/min arises from the blood vessels (12). Given these flow rates and the known geometry, we find Darcy's permeability of normal brain tissue (K^N) to be 6.4×10^{-15}m^2. While an experimental value for human brain tissue has not yet been reported, values for animal brain or other tissues vary widely between 1×10^{-19} and 1×10^{-14}m^2 (28–35). For rat brain tissue, K^N was found to be 2.2–3.5×10^{-15}m^2 (34,35). On the other hand, the hydraulic conductivity (L_p^N) is estimated to be 1.4×10^{-13}m/Pa·s, which is in reasonably good agreement with available values for human brain of 0.8–1.1×10^{-13}m/Pa·s (13,36). The result is also in accord with that for a single brain microvessel of frog pial, 2.1×10^{-13}m/Pa·s (37).

Brain Interstitial Pressure and Fluid Flow

The simulation results for pressure contours, velocity contours, and the direction of the velocity vector in normal brain tissue are shown in Fig. 4a and c. The interstitial fluid primarily flows from the ventricle (high pressure domain) to the brain periphery/*arrachnoid villi* (low pressure domain). The average (superficial) intracranial fluid velocity ($\mathbf{v}$) is 1.3×10^{-7}m/s, which corresponds to an interstitial velocity ($\mathbf{v}/\alpha^N$) of 6.5×10^{-7}m/s. This is in a good agreement with the normal magnitude of fluid velocity in brain of ~10^{-7}–10^{-6}m/s (12,20,21).

The fluid flow in the presence of tumor is rather different, since tumor is highly vascularized and relatively more permeable than normal tissue. Here, we assume L_p^T for the tumor to be 7.8-fold that of the normal tissue (L_p^N) (38), while K^T for the tumor is 10-fold that of normal tissue (K^N) (15). In addition, the vascular density of tumor (S/V^T) increases to 20,000 m^{-1} as compared to 7,000 m^{-1} for normal tissue (S/V^N) (15). The pressure and flow field results for a patient with *glioblastoma* are shown in Fig. 4b and d, respectively. The tumor has a higher mean pressure (1,182 Pa) than that of the same domain in the normal case (1,047 Pa) because hydraulic conductivity (L_p^T) and vascular density (S/V^T) are higher for tumor tissue. The pressure increase is modest because K^T is also much higher. Thus, the fluid in the tumor flows at higher velocity ($\mathbf{v} = 4.6 \times 10^{-7}$m/s), and most of the flow maintains its path toward the brain periphery. In reality, the interstitial pressure increase in human brain tumor is quite variable but is typically between 700 and 3,000 Pa (28). This can be caused by the variability in tumor size, the increase of L_p^T (which can be up to 100 times depending on the tumor type/malignancy), and S/V^T (15).

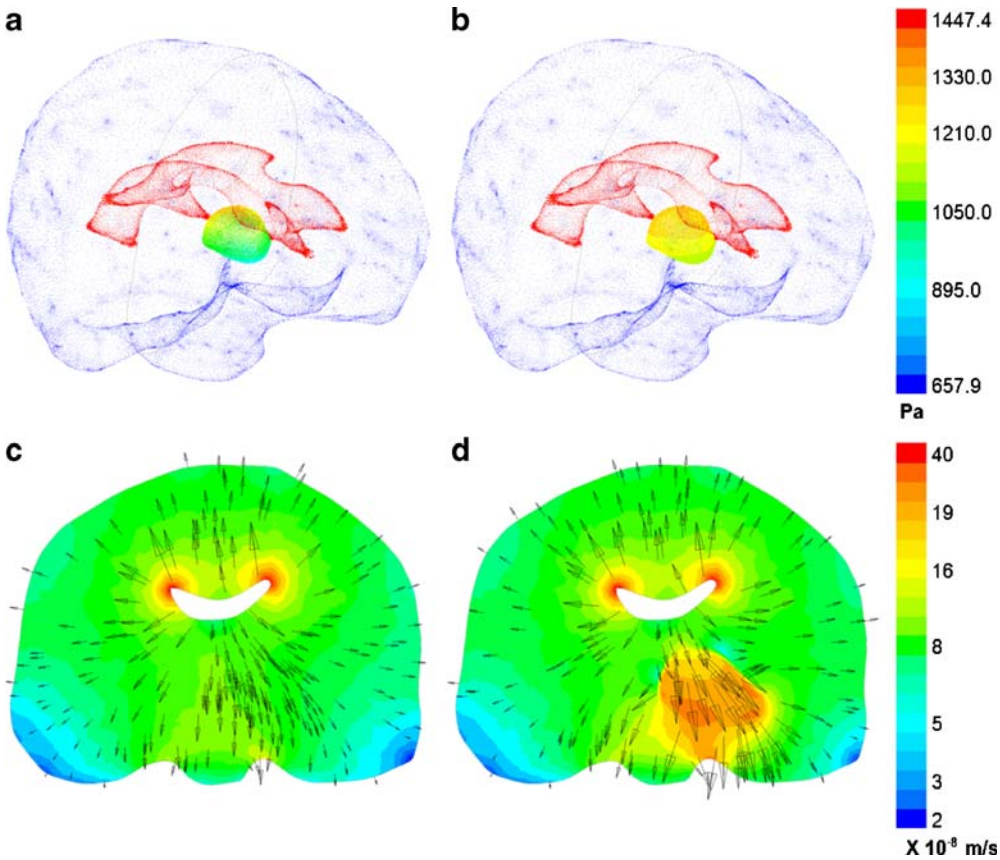

Fig. 4. The simulated interstitial fluid flow in human brain for normal and tumor cases; the 3D steady-state pressure contours of **a** normal and **b** tumor case; and the 2D-coronal steady-state velocity contours and vectors of **c** normal and **d** tumor case. Note increase in tumor interstitial fluid pressure (1,182 Pa) as compared to that of the same domain in normal tissue (1,047 Pa). Similarly, the fluid in the tumor flows at higher mean velocity ($\mathbf{v} = 4.6\times10^{-7}$m/s) as compared to that of the same domain in normal tissue ($\mathbf{v} = 1.3\times 10^{-7}$m/s), as shown in the respective velocity contour.

Treatment Model: Tumor Resection and Gliadel® Wafer Implantation

Before investigating the drug distribution to the remnant tumor, we first investigate the flow field in the treatment domain. The fluid flow is complex due to the presence of the surgical cavity and edema.

Interstitial Pressure and Fluid Flow in the Treatment Domain

Surgery causes brain trauma, which leads to edema, which is due to additional fluid production because blood vessels near the surgical cavity become very leaky (11,17). This is mathematically modeled as an increase in the hydraulic conductivity of the remnant tumor (L_p^T) as suggested by Eq. 3. In addition, the tumor removal introduces a new domain: the cavity. As the cavity is filled by cellulosic Surgicel, its permeability (K^C) is taken to be 1×10^{-11}m^2 (10,11). A sensitivity analysis in which K^C was varied between 1×10^{-12} and 1×10^{-10}m^2 resulted in no appreciable difference in the fluid flow, suggesting that tissue poses the controlling resistance.

Fig. 5 shows the interstitial fluid pressure contours as a function of time. The presence of edema immediately after the surgery gives rise to an increase of fluid pressure in the treatment domain. The mean fluid pressure in the cavity is 1,400 and 1,339 Pa at four and 8 h following the surgery, respectively, while that in the remnant tumor is 1,397 and 1,338 Pa. At Hour 24, the edema starts to be resolved as the hydraulic permeability in the tumor (L_p^T) has diminished to about 74% above the baseline; therefore, the fluid pressures in the cavity and tumor decrease to 1,191 and 1,190 Pa, respectively. From Hour 72 onwards, the cavity and tumor achieve a stable pressure of 1,108 Pa. This stable pressure is lower than when tumor is still present (1,182 Pa) and approaches that of normal brain pressure (1,047 Pa), suggesting that tumor removal surgery is indeed required to lower the brain fluid pressure. Note that high brain fluid pressure is often correlated with patient discomfort, seizures, etc.

Fig. 6 shows the two-dimensional (2D) interstitial fluid velocity vectors and contours inside the cavity at different times. The vectors show that the main direction of the interstitial flow is still from the ventricle to the brain periphery. The velocity magnitude in the cavity is always higher than in brain tissue (the volume-averaged $\mathbf{v} = 8 \times 10^{-7}$ m/s). For comparison, $\mathbf{v} = 1.3 \times 10^{-7}$m/s for normal brain tissue without tumor. This is due to the higher permeability of the cavity as compared to the tissue. Interestingly, the contours show that the spatial variation of velocity is quite significant ($\mathbf{v} = 5 \times 10^{-8}$–$3 \times 10^{-6}$m/s), as a result of the

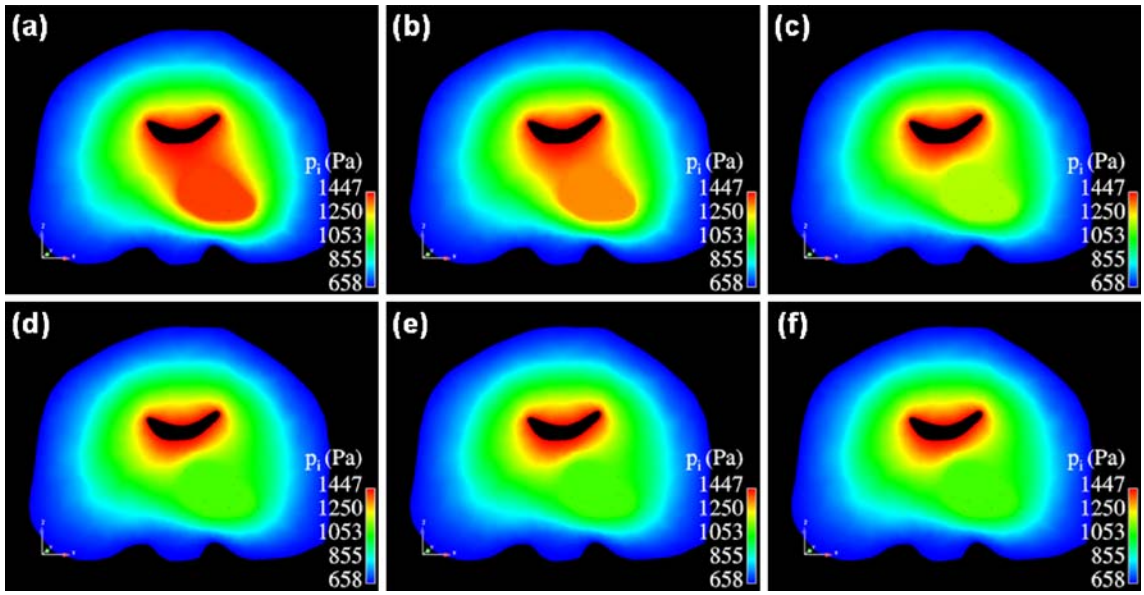

Fig. 5. Pressure contours shows how edema causes a sudden increase of pressure after tumor removal surgery: **a** Hour 4, **b** Hour 8, **c** Hour 24, **d** Hour 72, **e** Hour 120, and **f** Hour 168. The resolution starts at Hour 24 and is marked by the pressure decrease back to normal (Hour 72 onwards).

irregular shape of the cavity and of the wafers inside the cavity. In the absence of wafers, the velocity variation is from 3×10^{-7} to 2×10^{-6} m/s, suggesting that wafer implantation indeed widens the velocity distribution. On the other hand, the temporal variation is largely limited to the top left domain (near the ventricle), as shown as shown by the evolution from Hour 4 to Hour 72.

Since the model assigns edema solely to the remnant tumor, it is important to understand the variation of velocity in this region. In addition, the drug penetration to the remnant tumor begins at the cavity/remnant tumor interface; therefore, the convective flow towards (or away from) this interface requires special attention. Fig. 7 shows the magnitude of the fluid velocity on the cavity surface by color-coded contours. Direction is shown by the vectors. From the results, there are at least three different domains of special interest with different characteristics, located at the top left, top right, and bottom of the cavity surface. At the top left section, when

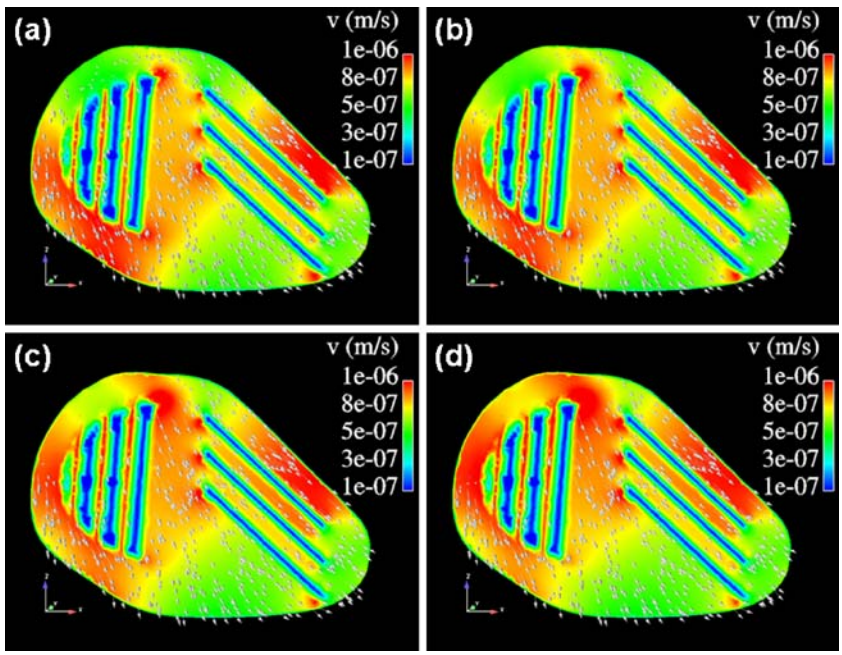

Fig. 6. The two-dimensional (2D) interstitial fluid velocity vectors and contours inside the cavity at different times: **a** Hour 4, **b** Hour 8, **c** Hour 24, and **d** Hour 72. The volume-averaged velocity magnitude in the cavity is always higher ($\mathbf{v} \sim 8 \times 10^{-7}$ m/s) than in brain tissue ($\mathbf{v} = 1.3 \times 10^{-7}$ m/s). Furthermore, the interstitial fluid mainly flows from the ventricle to the brain periphery.

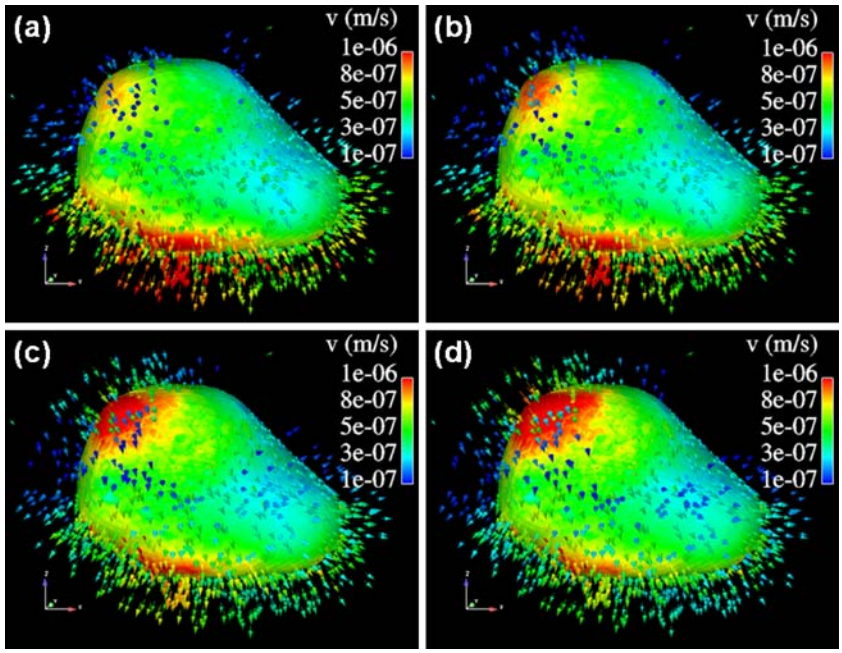

Fig. 7. The interstitial fluid velocity vectors during the edema: **a** Hour 4, **b** Hour 8, **c** Hour 24, and **d** Hour 72. There are at least three different domains of special interest with different flow characteristics, located at the *top left*, *top right*, and *bottom* of the cavity surface. After edema is resolved (Hour 24 onwards), at the *top left* section, the flow is dominantly into the cavity. At the *top right* of the tumor, the flow direction is aligned parallel to the cavity surface. At the *bottom* domain, the interstitial fluid streams outward from the cavity surface toward the brain periphery.

edema occurs, most of the fluid flows into the cavity. However, some fluid flows towards the ventricle at Hours 4 and 8; this occurs because permeation from the vasculature is elevated during edema. When edema resolves (Hours 24 and 72), fluid permeation in the tumor decreases. As a result, the pressure decreases and interstitial fluid flows into the cavity. At the top right of the tumor, the flow has a tendency to be aligned (parallel) to the cavity surface, following the normal pressure gradient. Even during the edema, a very small portion with relatively low velocity magnitude is directed normal to the surface. In contrast, at the bottom domain, the interstitial fluid streams outward from the cavity surface during the entire period. During edema, the velocities in this region are relatively high due to the additional contribution from the increased permeation from tumor capillaries, but they decrease as the edema resolves.

It is of interest to elucidate the behavior of the convective flow in these three domains in more detail. Accordingly, we study the velocity variation along the three representative lines, located at the top left, top right, and bottom of the cavity surface, as shown in Fig. 8a. Fig. 8b, c, and d, which depict the variation of the interstitial fluid velocity components (tangential and normal) along these lines. Each compares a case when edema is present (i.e. Hour 4) with one when edema has resolved (i.e. Hour 72). The dimensionless distance used in this analysis is $\xi = x/L_{\mathrm{d}}^{\mathrm{T}}$, where x is the distance from the cavity/remnant tumor interface. Note that $\xi = 0$ refers to the cavity/remnant tumor interface, while $\xi = 7.4$ approximately indicates the remnant tumor/nearby normal tissue interface. In general, along all three lines, the normal component of velocity is smoothly continuous across the cavity/remnant tumor interface, while the tangential component is nearly discontinuous. The velocity magnitude is always higher in the cavity than in the remnant tumor due to the difference in permeability as discussed before. In the remnant tumor, the normal velocity component tends to be larger than the tangential component. Along lines A and B, the normal velocity component in the remnant tumor is higher in the presence of edema. In both lines, the flow is directed outwards from the cavity to the tumor. In contrast, along line C, the flow is toward the cavity. During edema (Hour 4), $v = 0$ at about the outer edge of the remnant tumor. Thus, the normal component of the pressure gradient must also be zero at this point. Or, to say it slightly differently, this is the site of a local maximum in the pressure. When edema resolves (Hour 72), the pressure maximum disappears; consequently, along line C, fluid flows only toward the cavity and at a relatively high velocity. Since drug penetration is influenced primarily by the normal velocity component, three different characteristics are manifested: (i) substantial normal velocity along line A, providing an enhanced penetration, (ii) relatively low normal velocity along line B, suggesting that convection may not play a role, and (iii) substantial normal velocity opposed to the penetration direction along line C, providing repressed penetration. This will be addressed in detail later in the section on drug penetration to the remnant tumor.

Carmustine Distribution in the Cavity

The release profile for the Gliadel® wafers (see Fig. 9) is a major determinant of concentration in the cavity. Due to the

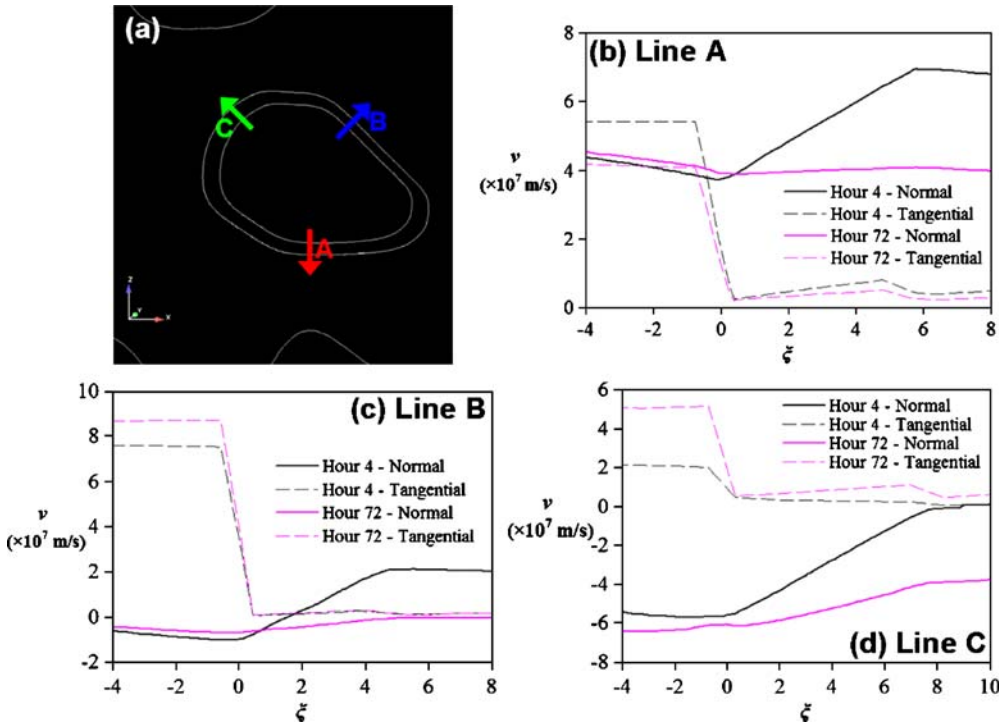

Fig. 8. The location of three representative lines under different influences of convective flow is shown in sub-figure (**a**). Line A refers to that with enhanced convection, B is that with minimal convection, while C is that with repressed convection. Sub-figures (**b**), (**c**), and (**d**) describe tangential and normal components of fluid velocity along lines A, B, and C, respectively. Each is shown for Hour 4 (when edema is present) and Hour 72 (when edema has mostly resolved). Along all three lines, the normal component of velocity is smoothly continuous across the cavity/remnant tumor interface, while the tangential component is nearly discontinuous.

initial burst, high concentration is present at 24 h post-implantation. The concentration is then modest up to about 120 h and is essentially zero at 168 h. Interestingly, at all times, the spatial variability is huge: as large as two orders of magnitude. Also, the drug distribution is aligned with the flow direction—high concentration is present in the downstream region (the bottom right part) of the cavity, and vice versa. It will be shown that this is mainly due to the convective flow.

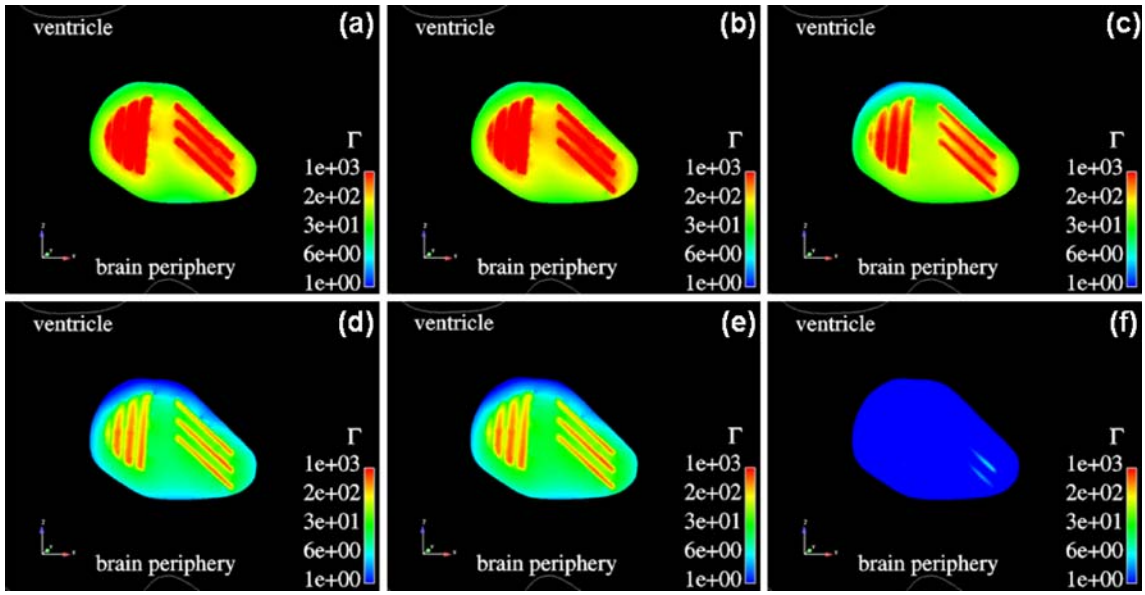

Fig. 9. The two-dimensional (2D) drug concentration (Γ) contour inside the cavity at different time points: (**a**) Hour 4, (**b**) Hour 8, (**c**) Hour 24, (**d**) Hour 72, (**e**) Hour 120, and (**f**) Hour 168. High drug concentration is observed at 24 h post-implantation because of the initial burst. The concentration is then modest up to about 120 h and is essentially zero at 168 h. At all times, the spatial variability inside the cavity is enormous: as about two orders of magnitude.

In the cavity, $\mathrm{Pe_c} = v_{s,c}L_c/D_i = 2$ and $\phi = L_c\sqrt{k_c/D_i} = 2.5$; thus, $\phi^2/\mathrm{Pe_c} = 3.1$. This latter quantity is the ratio of the time scale for convection across the cavity to that for reaction. In other words, convection is slow enough to permit a lot of reaction within the cavity. For this reason, we have constructed a simple one-dimensional model of the cavity which has only drug release, drug convection, and drug reaction. The drug release rate per unit volume (w) is assumed constant throughout the cavity; hence, the model can be simplified to a steady-state problem, which can be written as follows:

$$-v_{s,c}\frac{dC_i}{dx} + w - k_c C_i = 0 \tag{15}$$

where $v_{s,c} = 3 \times 10^{-7}$m/s is a constant fluid velocity within the cavity. The solution of the above equation for $C_i = 0$ at $x = 0$ is

$$C_i = (w/k_c)\left[1 - \exp\left(-k_c x/v_{s,c}\right)\right] \tag{16}$$

Thus, across the cavity length, the drug concentration will vary from zero to nearly w/k_c (=2.5×10^{-3}M, for instance, at Day 3). This value is comparable to the maximum value of concentration in the cavity (=3.2×10^{-3}M at Day 3) as predicted by the full model.

Carmustine Penetration to the Remnant Tumor

Fig. 10 shows the *carmustine* concentration on the cavity surface and in a coronal strip of remnant tumor and nearby tissue. There are at least three important messages which can be drawn from this series of contour plots. First, the *carmustine* release from Gliadel® wafers can provide therapeutic conditions (above $C_{i,eff}$ = 15 μM) only up to Hour 120, even at the cavity/remnant tumor interface. At Hour 168, the drug concentration has fallen well below the effective therapeutic concentration. This means that the drug release from Gliadel® wafers will not provide sufficient treatment beyond Hour 120. Second, at any given time, the concentration on the cavity surface varies by about two orders of magnitude. As discussed previously, this is mainly due to convection—with lower concentrations on the surfaces toward the ventricle and higher concentrations on surfaces directed away from the ventricle. Third, the penetration of the remnant tumor appears to be very limited, even at early times when drug concentration on the cavity surface is high. It is therefore important to understand the drug penetration mechanism in the presence of convective flow.

Table III quantifies the therapeutic penetration of *carmustine* along the three lines (A, B, and C) of Fig. 8a at different time points. The therapeutic penetration (TP—in mm) is defined as the length from the cavity/remnant tumor interface for which the drug concentration is above its therapeutic concentration ($C_{i,eff}$). For each of the three lines, TPs are highest during the period from Hour 8 to Hour 24. They decrease at Hours 72 and 120, and completely vanish at Hour 168. This confirms the expectation that the drug penetration should be strongly dependent on the drug release profile from the wafers. But, surprisingly, all of the TPs are less than the depth of the remnant tumor (L = 2.3 mm). Along line A, in which the penetration is enhanced by the convection, TPs are only of 1.1 and 1.2 mm at Hour 8 and 24, respectively, meaning that only half of the tumor thickness receives effective treatment. Along line B, drug infiltrates the tumor mainly by diffusion; thus, TPs are lower than those along line A for the same time point. Along line C, the penetration is repressed by the convection, and TPs are even lower than for the previous two lines.

In order to understand the preceding results, we turn to a simple one dimensional analysis under the assumption of

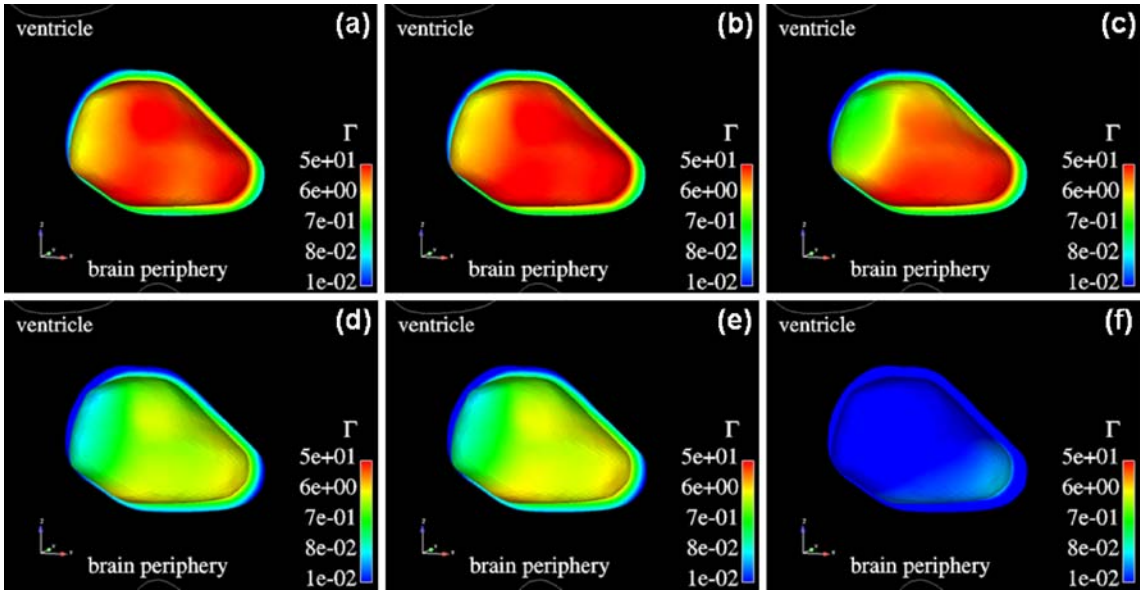

Fig. 10. The *carmustine* concentration (Γ) contours at: (**a**) Hour 4, (**b**) Hour 8, (**c**) Hour 24, (**d**) Hour 72, (**e**) Hour 120, and (**f**) Hour 168. Concentration contours are shown for the cavity surface and for a coronal strip of remnant tumor and nearby tissue. The *carmustine* concentration in the tumor reaches therapeutic conditions (Γ>1) only up to Hour 120. At Hour 168, its concentration is well below the effective therapeutic concentration (Γ<1).

Table III. The Therapeutic Penetration (TP—in mm) for Lines at Different Convective Regions as Depicted in Fig. 8. The Therapeutic Penetration is Defined as the Length from the Cavity/Remnant Tumor Interface in Which the Drug Concentration is Above its Therapeutic Concentration (for *carmustine*, $C_{i,eff}$ = 15 μM). The Mean Tumor Thickness (L) is 2.3 mm

Time Point	A	B	C
Hour 4	1.0	1.1	0.7
Hour 8	1.1	1.0	0.7
Hour 24	1.2	0.6	0.2
Hour 72	0.3	0.1	0.0
Hour 120	0.5	0.2	0.0
Hour 168	0.0	0.0	0.0

quasi-steady conditions. In this case, the domain of interest is that of the remnant tumor only, and Eq. 13 becomes

$$0 = \frac{d^2\Gamma_T}{d\xi^2} - \mathrm{Pe_t}\left(\frac{v_x}{v_s}\right)\frac{d\Gamma_T}{d\xi} - \Gamma_T \qquad (17)$$

where $\Gamma_T = C_i/C_{i,c}$ is the drug concentration normalized to that at the cavity/remnant tumor interface ($C_{i,c}$), and $\xi = x/L_d^T$ is the distance from the cavity/remnant tumor interface (x) normalized to the diffusion/reaction length scale in the tumor (L_d^T). The boundary conditions include (i) constant drug concentration at the cavity/remnant tumor interface surface ($\Gamma_T = 1$ at $\xi = 0$) and (ii) negligible drug concentration at infinity ($\Gamma_T = 0$ at $\xi = \infty$).

With a constant velocity (v_x), the solution is

$$\Gamma_T = \exp[-m\xi] \qquad (18)$$

where $m = \left(-\psi + \sqrt{1+\psi^2}\right)$ and $\psi = \left(v_x/\alpha^{*T}\right)/2\sqrt{k^T D^T}$. Small values of ψ mean that convection is not important for drug penetration, and vice versa. Note that, when the velocity is negligible ($v_x = 0$), the solution returns to that of the simple steady diffusion/reaction equation. If the fluid velocity is evaluated at the cavity surface, the values of ψ are 0.12, 0.02, and −0.18 for Lines A, B, and C, respectively. Fortunately, these values are very nearly independent of time (see Fig. 8).

Fig. 11 provides a comparison of the numerical solution with the analytical one (Eq. 18). Along line A, drug penetration is enhanced by convection—the penetration profile is stretched as compared to that for pure diffusion/reaction. Along the line B, the penetration more or less follows that for a diffusion/reaction model. In contrast, along the line C, the penetration is compressed due to the convection—the convective fluid flow is counter to the penetration direction. Nevertheless, even with the presence of enhanced/repressed convective flow, the concentration profiles deviate only very slightly from that for negligible convection. This suggests that the drug transport in the tumor is mainly by diffusion. It should also be noted that the numerical profiles for different times overlap each other, thereby justifying the assumption of quasi-steady behavior. However, the numerical results do lie somewhat above the analytical solutions at high penetration distances. This is because the simple model assumes the presence of tumor out to infinity. In the numerical case, there is a thick rim of normal tissue beyond the tumor. In the normal tissue, because the interstitial volume fraction is less, D^N is also less by about a factor of two. Thus, the normal tissue resembles an impermeable barrier which causes the numerical model to predict higher concentrations than does the analytical model. Nevertheless, the difference is small and the influence of convective flow can be predicted by Eq. 18 if the fluid velocity (v_x) at the cavity/remnant tumor interface is known.

Convection-Enhancement in Animal Experiments

It is useful to compare the results of this analysis with previous animal data. Previous modeling attempts for rat, rabbit, and monkey brain (20–22) have always assumed that the penetration should correspond to a simple diffusion/reaction model under quasi-steady conditions. But the models have always underestimated the experimental drug penetration distance. This is most likely because the drug penetration data were obtained by scanning the coronal section from the edge of the polymer to the brain periphery. Since flow in the brain is from the ventricle to the brain periphery, one could expect that the drug penetration would be influenced by enhanced convection. Note that all experiments were performed in a brain tissue without a tumor. Moreover, the incision was made to fit the placement of the implant; thus, no cavity was present. The penetration data for monkey brain (22) on Days 7, 14, and 30 are used for this analysis.

To examine the possible effect of convection, we used Eq. 18, but with parameter values which prevail in normal brain tissue instead of tumor, i.e. k^N and D^N for lumped first-order elimination constant and diffusivity in the normal tissue. In particular, $L_d^N = \sqrt{D^N/k^N} = 0.31$ mm and $\xi^N =$

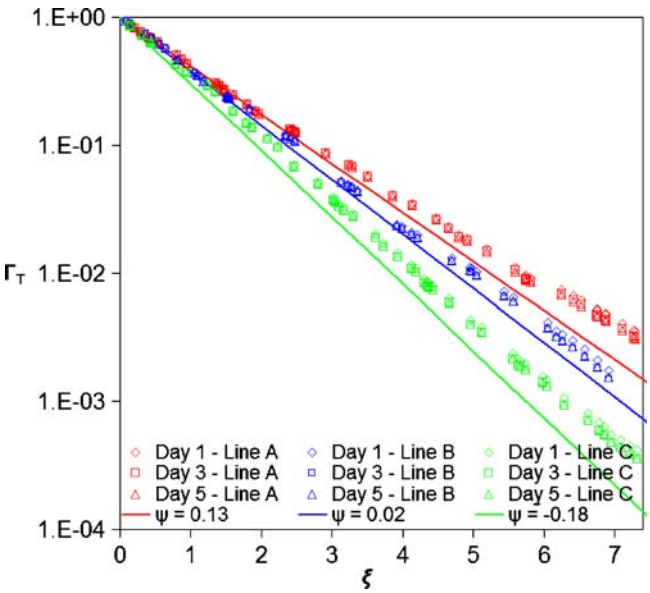

Fig. 11. The drug penetration profile from the cavity/remnant tumor interface along lines A, B, and C at different time points: Hour 24, Hour 72, and Hour 120. Along line A, the penetration is enhanced by convection—the penetration profile is stretched as compared to that for pure diffusion/reaction. Along line B, the penetration more or less follows that of the diffusion/reaction model. Along line C, the penetration is compressed due to the convection—the convective fluid flow is counter to the penetration direction.

x^N/L_d^N is the dimensionless distance from the pellet's surface (x^N). Also, note that Γ_N is the normalized concentration relative to the drug concentration on the surface of polymer pellet ($C_{i,c}^N$) as no cavity is present. The results shown in Fig. 12 support the hypothesis—fitted values of $\psi^N = (v_x/\alpha^{*N})/2\sqrt{k^N D^N}$ are found to lie between 0.8 and 2.2 in the monkey brain. This clearly implies the presence of convection. The drug penetration is more enhanced at Days 7 and 14 ($\psi^N = 2.2$) than at Day 30 ($\psi^N = 0.8$), suggesting that the influence of the convective flow is more important at Days 7 and 14 rather than at Day 30. This may suggest that the edema might still be present at Days 7 and 14 but that it had normalized at Day 30. It seems that severe edema in the monkey brain prevailed for long times, as indicated by high values of ψ^N (high fluid permeation from injured tissues) and long periods of resolution (more than 2 weeks). The reasons are unclear, though one might argue that surgery performed in a small animal might be even more traumatic than in a human. Nevertheless, it shows how convection can influence the drug penetration. Thus, a simple diffusion/reaction model might not be sufficient to explain drug distribution in the tissue, especially when the level of edema is significant.

Potential Alternative to *Carmustine*

Our previous discussion has suggested that a successful drug delivery system needs to be able to provide (a) sufficiently high concentration in the cavity and, subsequently, (b) adequate penetration to the remnant tumor. In this regard, *carmustine* fails to meet both criteria, limiting the penetration depth to less than few millimeters. This is related to the physico-chemical properties of the agent; therefore, potential replacement of *carmustine* is worth considering.

The efficacy of several chemotherapeutic agents against brain tumors is currently being investigated (39). Amongst them, *paclitaxel* is of particular interest from a transport perspective for the following reasons. First, it experiences much less degradation in the cavity ($k_c = 9.63 \times 10^{-5}$ 1/s, 22) than *carmustine* ($k_c = 6.79 \times 10^{-7}$ 1/s). In other words, its degradation half-life is much longer ($t_{1/2} = \ln(2)/k_c = 17{,}000$ min) than that of *carmustine* ($t_{1/2} = 120$ min). As a result, a much higher *paclitaxel* concentration is available in the cavity. Second, *paclitaxel* is capable of penetrating more deeply into the remnant tumor. Though its diffusivity ($D_i = 9 \times 10^{-4} m^2/s$) is similar to that of *carmustine*, it is much less subject to elimination via transcapillary exchange ($k_{bbb} = 1.39 \times 10^{-4}$ 1/s, 22) than *carmustine* ($k_{bbb} = 1.44 \times 10^{-2}$ 1/s). This is mainly because of the larger molecular size of *paclitaxel* ($M_w = 853.9$ kg/kmol) as compared with *carmustine* ($M_w = 214.1$ kg/kmol), constraining its escape passage through blood-brain barrier. It has been suggested that the molecular weight threshold for a compound to cross the BBB is 450 kg/kmol (40). Furthermore, as aforementioned, its degradation constant (k_c) is also less than that of *carmustine*. Consequently, as the dilution effect (F_V) is of minor significance, *paclitaxel* is characterized by a diffusion/reaction length scale ($L_d^T = 2.5$ mm) which is significantly greater than that of *carmustine* ($L_d^T = 0.31$ mm). In normal tissue, its length scale is similar, i.e. $L_d^N = 2.5$ mm. This is consistent with experimental data in normal rat brain (41) which showed that the *paclitaxel* concentration at about 4 mm from the polymeric implant (at Day 30 post-implantation) is between 8 and 24% (average of 16%) of the concentration at the centre of the implant.

Third, *paclitaxel* (log $P_{m/i} = 3.5$, 22) is much more hydrophobic than *carmustine* (log $P_{m/i} = 1.5$, 22), so it can be more conveniently and efficiently encapsulated in a wide variety of FDA-approved hydrophobic polymers, especially *poly(lactic-co-glycolic acid* (PLGA) family. The use of hydrophobic polymers avoids any major initial burst (42,43) and allows the controlled release to extend over a period of weeks to months. In contrast, devices based on hydrophilic polymers tend to have release periods of days (44). Thus, future studies involving *paclitaxel* as an alternative strategy against brain tumors are certainly worth exploring.

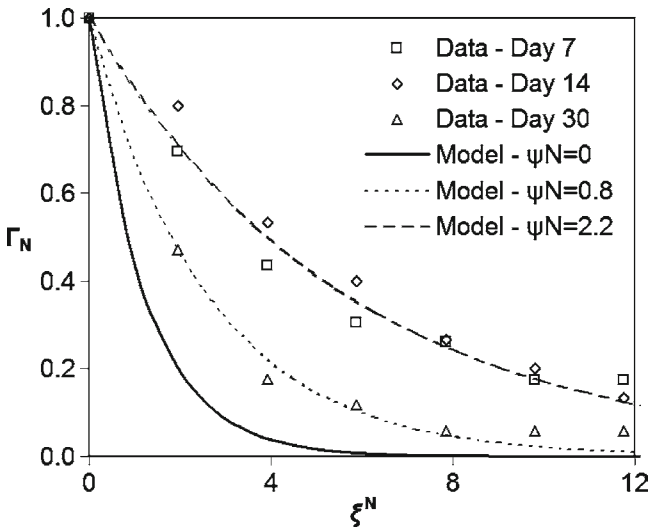

Fig. 12. The prediction of *carmustine* penetration in monkey brain via a simple one-dimensional model (Eq. 18) as compared to experimental data obtained in monkey brain (22). The drug penetration enhancement is greater at Days 7 and 14 ($\psi^N = 2.2$) than at Day 30 ($\psi^N = 0.8$). This implies that the effect of the convective flow (due to edema) is more crucial at Days 7 and 14 rather than at Day 30.

Clinical Implications

This study explores the important role that convective flow plays in distributing *carmustine* from a polymeric implant (Gliadel® wafers) to the remnant tumor. Though the penetration mechanism to the remnant tumor is dominated by diffusion, the influence of convective flow is important, especially in the cavity which is present as a result of the surgery. The remnant tumor located near the ventricle is exposed to very low drug concentrations due to convection which opposes diffusion, while that away from the ventricle is exposed at higher concentrations due to enhancement by convection. In any event, the effect of convective flow on drug penetration can be estimated by a simple analysis (Eq. 18), provided that the drug concentration at the cavity surface is known. To address this issue, hydraulically impermeable drug delivery devices could be placed directly on the cavity/remnant tumor interface to obviate the effect of convection in the cavity. An example of such a device might be an impervious film from which the drug would be released. Furthermore, the surgeon

needs to obtain the cleanest tumor incision possible, particularly in regions where convection opposes diffusion. In addition, it was found that, due to rapid transcapillary exchange, *carmustine* does not achieve adequate penetration of the remnant tumor. For this reason, other chemotherapeutic agents, for instance *paclitaxel*, could be more attractive.

ACKNOWLEDGMENTS

This work was supported by Biomedical Research Council (BMRC), A*STAR, Singapore and National University of Singapore under the grant number BMRC/07/1/21/19/508 (R-279-000-257-305). The authors thank the Supercomputing and Visualization Unit (SVU) of National University of Singapore for providing facilities to perform all the simulation works.

REFERENCES

1. Jemal A, Siegel R, Ward E, Xu J, Smigal C, *et al*. Cancer Statistics, 2006, CA. Cancer J Clin. 2006;56:106–30.
2. Berger MS, Bernstein M. Neuro-oncology: the essentials. New York: Thieme Medical; 2000.
3. Pardridge WM. The blood-brain barrier: bottleneck in brain drug delopment. Journal of the American Society for Experimental NeuroTherapeutics. 2005;2:3–14.
4. Huynh GH, Deen DF, Szoka FC Jr. Barriers to carrier mediated drug and gene delivery to brain tumors. J Control Release. 2006;110:236–59.
5. Heldin C-H, Rubin K, Pietras K, Ostman A. High interstitial fluid pressure—an obstacle in cancer therapy. Nat Rev Cancer. 2004;4:806–13.
6. Brem H, Gabikian P. Biodegradable polymer implants to treat brain tumors. J Control Release. 2001;74:63–7.
7. Westphal M, Ram Z, Riddle V, Hilt D, Bortey E, and On behalf of the Executive Committee of the Gliadel® Study Group. Gliadel® wafer in initial surgery for malignant glioma: long-term follow-up of a multicenter controlled trial. Acta Neurochir. 2006;148:269–75.
8. Giese A, Kucinski T, Knopp U, Goldbrunner R, Hamel W, Mehdorn HM, *et al*. Pattern of recurrence following local chemotherapy with biodegradable *carmustine* (BCNU) implants in patients with glioblastoma. J Neurooncol. 2004;66:351–60.
9. Wang CH, Li J, Teo CS, Lee T. The delivery of BCNU to brain tumors. J Control Release. 1999;61:21–41.
10. Tan KH, Wang FJ, Lee T, Wang CH. Delivery of *etanidazole* to brain tumor from PLGA wafers: a double burst release system. Biotechnol Bioeng. 2003;82:278–88.
11. Tan KH, Lee T, Wang CH. Simulation of intra-tumoral release of *etanidazole*: effects of the sized of surgical opening. J Pharm Sci. 2003;92:773–89.
12. Kimelberg HK. Water homeostasis in the brain: basic concepts. Neuroscience. 2004;120:852–60.
13. Rapoport SI. A mathematical model for vasogenic brain edema. J Theor Biol. 1978;74:439–67.
14. Gross JF, Popel AS. Mathematical models of transport phenomena in normal and neoplastic tissue. In: Peterson HI, editor. Tumor blood circulation. Baca Raton: CRC; 1979. p. 169–83.
15. Baxter LT, Jain RK. Transport of fluid and macromolecules in tumors. I. Role of interstitial pressure and convection. Microvasc Res. 1989;37:77–104.
16. Engelhard HH. The role of interstitial BCNU chemotherapy in the treatment of malignant glioma. Surg Neurol. 2000;53:458–64.
17. Nagashima T, Shirakuni T, Rapoport SI. A two-dimensional, finite element analysis of vasogenic brain edema. Neurol Med Chir (Tokyo). 1990;30:1–9.
18. Barzo P, Marmarou A, Fatouros P, Hayasaki K, Corwin F. Contribution of vasogenic and cellular edema to traumatic brain swelling measured by diffusion-weighted imaging. J Neurosurg. 1997;87:900–7.
19. Golan DE, Tashjian AH, Armstrong E, Galanter JM, Armstrong AW, Arnaout RA, *et al*. Principles of pharmacology: the pathophysiologic basis of drug therapy. Baltimore: Williams & Wilkins; 2008. p. 58–9.
20. Fleming AB, Saltzman WM. Pharmacokinetics of the *carmustine* implant. Clin Pharmacokinet. 2002;41:403–19.
21. Fung LK, Shin M, Tyler B, Brem H, Saltzman WM. Chemotherapeutic drugs released from polymers: distribution of 1, 3-bis (2-chloroethyl)-1-nitrosurea in the rat brain. Pharm Res. 1996;13:671–82.
22. Fung LK, Ewend MG, Silis A, Sipos EP, Thompson R, Watts M, *et al*. Pharmacokinetics of interstitial delivery of *carmustine*, 4-*hydroperoxycyclophospamide*, and *paclitaxel* from a biodegradable polymer implant in the monkey brain. Cancer Res. 1998;58:672–84.
23. Saltzman WM, Radomsky ML. Drugs released from polymers: diffusion and elimination in brain tissue. Chem Eng Sci. 1991;46:2429–44.
24. Perry RH, editor. Perry's chemical engineers' handbook. New York: McGraw-Hill; 1997. p. 59–71.
25. Kalyansundaram S, Calhoun VD, Leong KW. A finite element model for predicting the distribution of drugs delivered intracranially to the brain. Am J Physiol Regul Integr Comp Physiol. 1997;42:R1810–21.
26. Goodman Gilman A, Rall RW, Nies AS, Taylor P. Goodman and Gilman's The Pharmacological Basis of Therapeutics. 8th ed. New York: Pergamon; 1990. p. 1221.
27. Deen WM. Analysis of Transport Phenomena. New York: Oxford University Press; 1998. p. 181–4.
28. Netti PA, Travascio F, Jain RK. Coupled macromolecular transport and gel mechanics: poroviscoelastic approach. AIChE Journal. 2003;49:1580–96.
29. Jain RK. Transport of molecules in the tumor interstitium: a review. Cancer Res. 1987;47:3039–51.
30. Boucher Y, Brekken C, Netti PA, Baxter LT, Jain RK. Intratumoral infusion of fluid: estimation of hydraulic conductivity and implications for the delivery of therapeutic agents. Br J Cancer. 1998;78:1442–8.
31. Johnson EM, Deen WM. Hydraulic permeability of agarose gel. AIChE Journal. 1996;42:1220–4.
32. Swabb EA, Wei J, Gullino PM. Diffusion and convection in normal and neoplastic tissues. Cancer Res. 1974;34:2814–22.
33. Neeves KB, Lo CT, Foley CP, Saltzman WM, Olbricht WL. Fabrication and characterization of microfluidic probes for convection enhanced delivery. J Control Release. 2006;111:252–62.
34. Bobo RH, Laske DW, Akbasak A, Morrison PF, Dedrick RL, Oldfield EH. Convection-enhanced delivery of macromolecules in the brain. Proc Natl Acad Sci U S A. 1994;91:2076–80.
35. Basser PJ. Interstitial pressure, volume, and flow during infusion into brain tissue. Microvasc Res. 1992;44:143–65.
36. Paulson OB, Hertz MM, Bolwig TG, Lassen NA. Filtration and diffusion of water across the blood-brain barrier in man. Microvasc Res. 1977;13:113–24.
37. Fraser PA, Dallas AD. Measurement of filtration coefficient cerebral microvessels of the frog. J Physiol. 1990;423:343–61.
38. Gerlowski LE, Jain RK. Microvascular permeability of normal and neoplastic tissues. Microvasc Res. 1986;31:288–305.
39. Wang PP, Frazier J, Brem H. Local delivery to the brain. Adv Drug Deliv Rev. 2002;54:987–1013.
40. Bickel U. How to measure drug transport across the blood-brain barrier. NeuroRX. 2005;2:15–26.
41. Li KW, Dang W, Tyler BM, Troiano G, Tihan T, Brem H, *et al*. Polifocate microshperes for paclitaxel delivery to central nervous system malignancies. Clin Cancer Res. 2003;9:3441–7.
42. Lee LY, Wang CH, Smith KA. Supercritical antisolvent production of biodegradable micro- and nanoparticles for controlled delivery of *paclitaxel*. J Control Release. 2008;125:96–106.
43. Ranganath SH, Wang CH. Biodegradable microfiber implants delivering *paclitaxel* for post-surgical chemotherapy against malignant *glioma*. Biomaterials. 2008;29:2996–3003.
44. Arifin DY, Lee LY, Wang CH. Mathematical modeling and simulation of drug release from microspheres: Implications to drug delivery systems. Adv Drug Deliv Rev. 2006;58:1274–325.